A theory of amorphous polymeric solids undergoing large deformations: application to micro-indentation of poly(methyl methacrylate)

N. M. AMES and L. ANAND
Department of Mechanical Engineering
Massachusetts Institute of Technology
Cambridge, MA 02139, USA

***Abstract*— Although existing continuum models for the elasto-viscoplastic response of amorphous polymeric materials phenomenologically capture the *large deformation* response of these materials in a reasonably acceptable manner, they do not adequately account for the *creep* response of these materials at stress levels below those causing "macro-yield", as well as the Bauschinger-type reverse yielding phenomena at strain levels less than $\approx 30\%$ associated with the macro-yield transient. Anand [1] has recently generalized the model of Anand and Gurtin [2] to begin to capture these important aspects of the mechanical response of such materials. In this work, we summarize Anand's constitutive model and apply it to the amorphous polymeric solid poly(methyl methacrylate) (PMMA), at ambient temperature and compressive stress states under which this material does not exhibit crazing. We describe our compression-tension and creep experiments on this material from which the material parameters in the model were determined. We have implemented the constitutive model in the finite-element computer program ABAQUS/Explicit [3], and using this finite-element program, we show numerical results for some representative problems in micro-indentation of PMMA, and compare them against corresponding results from physical experiments. The overall predictions of the details of the load, P, versus depth of indentaion, h, curves are very encouraging.**

***Index Terms*— Polymers, viscoplasticity, PMMA, micro-indentation.**

I. Introduction

OVER the past twenty years a significant advance in continuum-level modeling of the plastic deformation of amorphous polymers has been made by Parks, Argon, Boyce, Arruda, and their co-workers [4]–[6], and by Wu & van der Giessen [7]. Recently, Anand and Gurtin [2] have generalized the work of these authors and developed a *frame-indifferent and thermodynamically-consistent* theory for the plasticity of amorphous polymers under isothermal conditions below their *glass transition temperatures*. Although these models phenomenologically capture the *large deformation elastic-viscoplastic* response of these materials in a reasonably acceptable manner, they do not adequately account for the *creep* response of these materials at stress levels below those causing "macro-yield", as well as the Bauschinger-type reverse yielding phenomena at strain levels less than $\approx 30\%$ associated with the macro-yield transient. A reasonable model for the "small-strain" ($\lessapprox 30\%$) viscoelastic response is of importance to describe the structural response of components made from these materials.

Anand [1] has recently generalized the model of Anand and Gurtin [2] to begin to capture important aspects of the complex mechanical response associated with the macro-yield transient of these materials. Anand's theory is based on the mathematical approach and physical ideas contained in [2] and, following these authors, he also utilizes the Kröner [8]-Lee [9] decomposition, $\mathbf{F} = \mathbf{F}^e\mathbf{F}^p$, of the deformation gradient $\mathbf{F}$ into elastic and plastic parts, $\mathbf{F}^e$ and $\mathbf{F}^p$, and also assumes that the plastic flow is irrotational $\mathbf{W}^p = \mathbf{0}$, so that the evolution equation for $\mathbf{F}^p$ is $\dot{\mathbf{F}}^p = \mathbf{D}^p\mathbf{F}^p$, with $\mathbf{D}^p$ deviatoric. However, as a departure from the previous theory he assumes further that $\mathbf{D}^p$ is given by the sum of $N+1$ micro-mechanisms, such that $\mathbf{D}^p = \sum_{\alpha=0}^{N} \mathbf{D}^{p\,(\alpha)}$. He chooses the inelastic micro-mechanism indexed by $\alpha = 0$ to represent the dominant "macro-yield" response, while the inelastic micro-mechanisms indexed by $\alpha = 1, \ldots, N$ are chosen to represent the finer details of the "viscoelastic" response of the material associated with the macro-yield transient. Correspondingly, he introduces $\boldsymbol{\sigma} = (s^{(0)}, s^{(1)}, s^{(2)}, \ldots, s^{(N)})$, a list of (N+1) positive-valued scalar fields, and another list of (N+1) symmetric tensor fields $\boldsymbol{\mathcal{A}} = (\mathbf{A}^{(0)}, \mathbf{A}^{(1)}, \mathbf{A}^{(2)}, \ldots, \mathbf{A}^{(N)})$, that represent aspects of the intermolecular resistances to plastic flow associated with each inelastic micro-mechanism. Further,

SMA Fellow AMMNS and IMST Programmes; E-mail:anand@mit.edu

since a key feature controlling the macro-yield of amorphous materials is known to be the evolution of the local free-volume associated with the metastable state of these materials, he also utilizes a scalar internal variable φ that represents the local free-volume. Introduction of these internal-state variables allows the model to phenomenologically capture important aspects of the creep response of solid polymers prior to macro-yield, as well as the highly non-linear stress-strain behavior that precedes the yield-peak and gives rise to post-yield strain-softening. Anand's theory explicitly accounts for the dependence of the Helmholtz free energy on the tensorial internal state variables in a thermodynamically-consistent manner. This dependence leads directly to backstresses in the underlying flow rule, and allows the model to capture aspects of the strong Bauschinger-type reverse-yielding phenomena typically observed in amorphous polymeric solids upon unloading after inelastic deformations.

The plan of this paper is as follows. We summarize Anand's [1] three-dimensional constitutive theory in Section II. In Section III we apply this model to the amorphous polymeric solid poly(methyl methacrylate) (PMMA). We describe our compression-tension and creep experiments at ambient temperature and stress states under which this material does not exhibit crazing; these experiments were used to calibrate the material parameters in the constitutive model. We have implemented the constitutive model in the finite-element computer program ABAQUS/Explicit [3], and using this finite-element program, in Section IV we show numerical results for some representative problems in micro-indentation, and compare them against corresponding results from physical experiments. We close in Section V with some final remarks.

NOTATION

∇ and Div denote the gradient and divergence with respect to the material point $\mathbf{X}$ in the *reference configuration*; grad and div denote these operators with respect to the point $\mathbf{x} = \mathbf{y}(\mathbf{X}, t)$ in the deformed configuration; a superposed dot denotes the material time-derivative. Thus, $\mathbf{F} = \nabla \mathbf{y}$ is the deformation gradient. Throughout, we write $\mathbf{F}^{e-1} = (\mathbf{F}^e)^{-1}$, $\mathbf{F}^{p-\top} = (\mathbf{F}^p)^{-\top}$, etc. We write $\operatorname{sym}\mathbf{A}$, $\operatorname{skw}\mathbf{A}$, $\mathbf{A}_0$, and $\operatorname{sym}_0\mathbf{A}$ respectively, for the symmetric, skew, deviatoric, and symmetric-deviatoric parts of a tensor $\mathbf{A}$. Also, the inner product of tensors $\mathbf{A}$ and $\mathbf{B}$ is denoted by $\mathbf{A}\cdot\mathbf{B}$, and the magnitude of $\mathbf{A}$ by $|\mathbf{A}| = \sqrt{\mathbf{A}\cdot\mathbf{A}}$.

II. CONSTITUTIVE MODEL FOR AMORPHOUS POLYMERS

The underlying constitutive equations relate the following basic fields:

ψ,	free energy density per unit volume of relaxed configuration,
$\mathbf{T}$, $\quad \mathbf{T} = \mathbf{T}^\top$,	Cauchy stress,
$\mathbf{F}$, $\quad J = \det\mathbf{F} > 0$,	deformation gradient,
$\mathbf{F}^p$, $\quad \det\mathbf{F}^p = 1$,	plastic def. gradient,
$\mathbf{F}^e = \mathbf{F}\mathbf{F}^{p-1}$, $\quad \det\mathbf{F}^e > 0$	elastic def. gradient,
$\mathbf{F}^e = \mathbf{R}^e\mathbf{U}^e$,	polar decomp. of $\mathbf{F}^e$,
$\mathbf{U}^e = \sum_{\alpha=1}^{3} \lambda^e_\alpha \mathbf{r}_\alpha \otimes \mathbf{r}_\alpha$,	spectral decomp. of $\mathbf{U}^e$,
$\mathbf{E}^e = \sum_{\alpha=1}^{3} (\ln\lambda^e_\alpha)\mathbf{r}_\alpha \otimes \mathbf{r}_\alpha$,	logarithmic elastic strain,
$\mathbf{F}^* = J^{-1/3}\mathbf{F}$,	distortional part of $\mathbf{F}$,
$\mathbf{C}^* = \mathbf{F}^{*\top}\mathbf{F}^*$,	right Cauchy-green tensor corresponding to $\mathbf{F}^*$,
$\mathbf{B}^* = \mathbf{F}^*\mathbf{F}^{*\top}$,	left Cauchy-green tensor corresponding to $\mathbf{F}^*$,
$\boldsymbol{\mathcal{A}} = (\mathbf{A}^{(0)}, \ldots, \mathbf{A}^{(N)})$, $\mathbf{A}^{(\alpha)} = \mathbf{A}^{(\alpha)\top}$,	symmetric tensor internal variables,
$\boldsymbol{\sigma} = (s^{(0)}, \ldots, s^{(N)})$, $s^{(\alpha)} > 0$,	scalar internal variables,
φ,	internal variable representing free volume.

The special set of constitutive equations is summarized below:

1) **Free Energy**:

$$\psi = \psi^e(\mathbf{E}^e) + \Psi(\mathbf{C}^*) + \sum_{\alpha=0}^{N} \xi^\alpha(\mathbf{A}^{(\alpha)}, \varphi). \quad (1)$$

Here,

$$\psi^e = G|\mathbf{E}^e_0|^2 + \tfrac{1}{2}K|\operatorname{tr}\mathbf{E}^e|^2, \quad (2)$$

where $G > 0$ and $K > 0$ are the elastic shear and bulk moduli, respectively.

For $\Psi(\mathbf{C}^*)$ we define an *effective (distortional) stretch*

$$\bar{\lambda} \stackrel{\text{def}}{=} \tfrac{1}{\sqrt{3}}\sqrt{\operatorname{tr}\mathbf{C}^*}, \quad (3)$$

and adopt the *Langevin-inverse* form

$$\Psi = \mu_R\,\lambda_L^2\left[\left(\frac{\bar{\lambda}}{\lambda_L}\right)x + \ln\left(\frac{x}{\sinh x}\right) - \left(\frac{1}{\lambda_L}\right)y - \ln\left(\frac{y}{\sinh y}\right)\right], \quad (4)$$

$$x = \mathcal{L}^{-1}\left(\frac{\bar{\lambda}}{\lambda_L}\right), \qquad y = \mathcal{L}^{-1}\left(\frac{1}{\lambda_L}\right), \quad (5)$$

where $\mathcal{L}^{-1}$ is the inverse of the Langevin function $\mathcal{L}(\ldots) = \coth(\ldots) - (\ldots)^{-1}$. The material parameter μ_R is called the *rubbery modulus*, and λ_L is called the *network locking stretch*.

For the free energies $\xi^\alpha(\mathbf{A}^{(\alpha)}, \varphi)$ we define *effective stretches*

$$\lambda^{(\alpha)} \stackrel{\text{def}}{=} \tfrac{1}{\sqrt{3}}\sqrt{\operatorname{tr}\mathbf{A}^{(\alpha)}}, \tag{6}$$

and adopt the simple *neo-Hookean* form

$$\xi^\alpha = \mu^{(\alpha)}\,\frac{3}{2}\left\{\left(\lambda^{(\alpha)}\right)^2 - 1\right\} \tag{7}$$

$$\mu^{(\alpha)} = \hat{\mu}^{(\alpha)}(\varphi), \quad \alpha = 0, \ldots, N; \tag{8}$$

the material parameters $\mu^{(\alpha)}$, which are assumed to be functions of the free-volume φ, are called *back stress moduli*.

2) **Equation for the stress**:

$$\mathbf{T} = \mathbf{T}_A + \mathbf{T}_B, \tag{9}$$

with

$$\left.\begin{aligned} \mathbf{T}_A &= J^{-1}\mathbf{R}^e\left(\mathbf{S}_A^e\right)\mathbf{R}^{e\top} \\ \mathbf{S}_A^e &= 2G\mathbf{E}_0^e + K(\operatorname{tr}\mathbf{E}^e)\mathbf{1}, \end{aligned}\right\} \tag{10}$$

and

$$\left.\begin{aligned} \mathbf{T}_B &= J^{-1}\mu_B\mathbf{B}_0^*, \\ \mu_B &= \mu_R\left(\frac{\lambda_L}{3\bar{\lambda}}\right)\mathcal{L}^{-1}\left(\frac{\bar{\lambda}}{\lambda_L}\right). \end{aligned}\right\} \tag{11}$$

3) **Equations for the backstresses**:

$$\mathbf{S}_{\text{back}}^{(\alpha)} = \mu^{(\alpha)}\mathbf{A}^{(\alpha)}, \qquad \alpha = 0, \ldots, N. \tag{12}$$

4) **Flow rule**:

$$\dot{\mathbf{F}}^p = \mathbf{D}^p\mathbf{F}^p, \qquad \mathbf{F}^p(\mathbf{X}, 0) = \mathbf{1}, \tag{13}$$

with $\mathbf{D}^p$ given by the sum of plastic stretchings from $(N+1)$ micro-mechanisms

$$\left.\begin{aligned} \mathbf{D}^p &= \sum_{\alpha=0}^{N} \nu^{(\alpha)}\left(\frac{(\mathbf{S}_A^e)_0 - (\mathbf{S}_{\text{back}}^{(\alpha)})_0}{2\bar{\tau}^{(\alpha)}}\right), \\ \nu^{(\alpha)} &= \nu_0\left(\frac{\bar{\tau}^{(\alpha)}}{s^{(\alpha)} + \alpha_p^{(\alpha)}\pi}\right)^{\frac{1}{m^{(\alpha)}}}, \end{aligned}\right\} \tag{14}$$

where

$$\bar{\tau}^{(\alpha)} = \frac{1}{\sqrt{2}}\,|(\mathbf{S}_A^e)_0 - (\mathbf{S}_{\text{back}}^{(\alpha)})_0|, \tag{15}$$

is an *equivalent shear stress* for each micro-mechanism, and

$$\pi = -\frac{1}{3}\operatorname{tr}\mathbf{S}_A^e, \tag{16}$$

is a mean normal pressure. The quantity $\nu^{(\alpha)}$ is an *equivalent plastic shear strain rate* for the αth micro-mechanism, and is taken in a simple power law form, with ν_0 a *reference plastic shear strain rate*, and $0 < m^{(\alpha)} \le 1$ are *strain rate sensitivity parameters*. The limit $m^{(\alpha)} \to 0$ corresponds to the rate-independent limit, while $m^{(\alpha)} = 1$ corresponds to the linearly-viscous limit. Also, $\alpha_p^{(\alpha)}$ are *pressure sensitivity* parameters for each micro-mechanism.

5) **Evolution equation for the internal variables $\mathbf{A}^{(\alpha)}$**:

These are taken as

$$\left.\begin{aligned} \dot{\mathbf{A}}^{(\alpha)} &= \mathbf{D}^{p(\alpha)}\mathbf{A}^{(\alpha)} + \mathbf{A}^{(\alpha)}\mathbf{D}^{p(\alpha)}, \\ \mathbf{A}^{(\alpha)}(\mathbf{X}, 0) &= \mathbf{1}. \end{aligned}\right\} \tag{17}$$

6) **Evolution equations for the scalar internal variables $s^{(\alpha)}$ and φ**:

We consider the evolution equations for $s^{(0)}$ and φ in the special coupled rate-independent form

$$\left.\begin{aligned} \dot{s}^{(0)} &= h_0\left(1 - \frac{s^{(0)}}{\tilde{s}^{(0)}(\varphi)}\right)\nu^{(0)}, \\ \dot{\varphi} &= g_0\left(\frac{s^{(0)}}{s_{\text{cv}}^{(0)}} - 1\right)\nu^{(0)}, \end{aligned}\right\} \tag{18}$$

with

$$\tilde{s}^{(0)}(\varphi) = s_{\text{cv}}^{(0)}[1 + b(\varphi_{\text{cv}} - \varphi)], \tag{19}$$

where $\{h_0, g_0, s_{\text{cv}}^{(0)}, b, \varphi_{\text{cv}}\}$ are additional material parameters. The initial values of $s^{(0)}$ and φ are denoted by

$$s_i^{(0)} \qquad \text{and} \qquad \varphi_i.$$

The remaining scalar internal variables $s^{(\alpha)}$ are assumed to be *constants*:

$$s^{(\alpha)} = s_i^{(\alpha)}, \qquad \alpha = 1, \ldots, N. \tag{20}$$

where $s_i^{(\alpha)}$ denote their initial values.

7) **Evolution equations for backstress moduli**:

Finally, the backstress moduli $\mu^{(\alpha)}$ are taken to evolve with the free-volume φ according to

$$\left.\begin{aligned} \dot{\mu}^{(\alpha)} &= c^{(\alpha)}\left(1 - \frac{\mu^{(\alpha)}}{\mu_{\text{sat}}^{(\alpha)}}\right)\dot{\varphi}, \\ \mu^{(\alpha)}(\phi_i) &= \mu_i^{(\alpha)} \end{aligned}\right\} \tag{21}$$

where $\mu_i^{(\alpha)}$ are the initial values of $\mu^{(\alpha)}$ when φ is equal to its initial value φ_i, while $c^{(\alpha)} > 0$, and $\mu_{\text{sat}}^{(\alpha)} > 0$ are material constants for each α. We expect that $\mu_{\text{sat}}^{(\alpha)} \le \mu_i^{(\alpha)}$, so that $\mu^{(\alpha)}$ decreases to its final value $\mu_{\text{sat}}^{(\alpha)}$ as φ increases.

To complete the constitutive model for a particular amorphous polymeric material the constitutive parameter/functions that need to be specified are

$$\Big\{G, K, \mu_R, \lambda_L, \nu_0, m^{(\alpha)}, \alpha_p^{(\alpha)}, h_0, g_0, \\ s_{\text{cv}}^{(0)}, b, \varphi_{\text{cv}}, s_i^{(0)}, \varphi_i, s_i^{(\alpha)}, \mu_i^{(\alpha)}, c^{(\alpha)}, \mu_{\text{sat}}^{(\alpha)}\Big\} \ .$$

The number of material parameters scales with the number of assumed micromechanisms α, and as we shall see, this number can get large if one wishes to accurately reproduce the mechanical response of the material.

We have implemented our constitutive model in the finite-element computer program ABAQUS/Explicit [3] by writing a user material subroutine.

III. Material parameters for PMMA

We have applied the constitutive model to capture the salient features of the mechanical response of the amorphous polymeric solid poly(methyl methacrylate) (PMMA), in an initially well-annealed condition.[1] We have conducted compression-tension strain-controlled experiments,[2] as well as stress-controlled creep experiments in stress states under which this material does not exhibit crazing; these experiments were used to calibrate the material parameters in the constitutive model. The complete sample preparation details as well as the details of the experimental procedures may be found in [11].

A typical true stress versus true train curve for PMMA in monotonic simple compression to a compressive strain of 100%, followed by an unloading to zero stress, taken from Hasan [10], is shown in Fig. 1; compressive stresses and strains are plotted as positive. After an initial approximately linear region, the stress-strain curve becomes markedly nonlinear prior to reaching a peak in the stress at a strain of approximately 8%. The material then strain-softens until a minimum in stress is reached at a strain of approximately 30%. After this, the material exhibits a broad region of rapid strain hardening, as the stress once again rises because of the alignment and locking of the polymer chains. The unloading curve after 100% compressive strain shows a Bauschinger-like phenomenon.

Results for tests in which the specimens are first deformed to various strain levels up to 20% in simple compression, followed by change in straining direction to tension, are shown in Fig. 2; each curve represents a separate experiment, and as before, compressive stresses and strains are plotted as positive.[3] It is important to note the very sharp change in the shape of the unloading portion of the stress-strain curves, especially as the material transitions into the tension regime. This is evidence of the presence of strong internal stresses leading to the strong Bauschinger-like phenomenon at the macroscopic level. Since the total strain levels in these curves are quite small, $\leq 20\%$, the origin of these strong internal stresses is *not due to the internal stresses generated due to stretching and locking of the polymer chains*, which becomes significant only at the strain levels larger than about 75%.

Finally, Fig. 3 presents strain-time results from creep tests that were carried out at stress levels of 24 MPa, 50 MPa, 63 MPa, and 75 MPa which are *below the stress level of approximately* 110 MPa *corresponding to macro-yield*. Note that for the creep experiment at a stress level of 75 MPa, one obtains a creep strain of as much as 6% after one hour, and this is under conditions for which the material is stressed to a state well below its macro-yield point!

The material parameters in the constitutive model were obtained by fitting the model to these experiments. Our judicious (but heuristic) fitting procedure yields the following set of material parameters:[4]

$G = 1.58$ GPa	$K = 4.12$ GPa	$\mu_{\text{R}} = 15$ MPa
$\lambda_{\text{L}} = 1.7$	$\mu_i^{(0)} = 0$ GPa	$\mu_i^{(1,2,3)} = 3.5$ GPa
$\mu_{\text{cv}}^{(0)} = 0$ GPa	$\mu_{\text{cv}}^{(1)} = 1.1$ GPa	$\mu_{\text{cv}}^{(2)} = 0.4$ GPa
$\mu_{\text{cv}}^{(3)} = 0.2$ GPa	$s_i^{(0)} = 45$ MPa	$s_i^{(1)} = 15$ MPa
$s_i^{(2)} = 25$ MPa	$s_i^{(3)} = 35$ MPa	$s_{\text{cv}}^{(0)} = 36$ MPa
$c^{(1)} = 4.5$ GPa	$c^{(2)} = 1.8$ GPa	$c^{(3)} = 1.3$ GPa
$\nu_0 = 0.0005$	$h_0 = 4$ GPa	$g_0 = 0.012$
$b = 850$	$\varphi_i = 0$	$\varphi_{\text{cv}} = 0.001$
$m^{(0)} = 0.085$	$m^{(1,2,3)} = 0.18$	$\alpha_{\text{p}} = 0.204$

Comparison of this numerically calculated material response using this set of material parameters against corresponding experiments is shown for large-strain simple compression in Fig. 4, for moderate strain compression in Fig. 5, and creep in Fig. 6. To the best of our knowledge, all previous constitutive models for amorphous polymers are able to only adequately capture the large strain response shown in Fig. 4, but are unable to capture the smaller strain compression-tension response,

[1] As is well known, the mechanical response of amorphous thermoplastics is very sensitive to prior thermo-mechanical processing history. Our experiments were conducted on PMMA specimens which were annealed at the glass transition temperature of this material, 105°C, for 2 hours, and then furnace-cooled to room temperature in approximately 15 hours. The experiments reported here were conducted under isothermal conditions at room temperature.

[2] All experiments were conducted at an absolute value of strain rate of 0.0003 s^{-1}, except for the experimental stress-strain curve in Fig. 1, from Hasan [10], which was conducted at a strain rate of 0.001 s^{-1}.

[3] The tensile stress levels to which the specimens were subjected were restricted such that they were not enough to initiate crazing.

[4] The steps and guidelines used in the fitting procedure are detailed in [11].

as well as the creep response at pre-peak stress levels. In contrast, the versatility of our new constitutive model is highlighted by its capability to obtain very reasonable fits for all three diverse loading cases.

As noted previously, the list of material parameters in our theory *is rather large*, but a large number of material parameters is needed to describe the complexity of the material response shown in Fig. 4 to Fig. 6. We also note the values of material parameters determined by our heuristic procedure is not unique; however, this non-uniqueness is not of substantial significance for demonstrating the major features predicted by the theory.

In the next section we apply the constitutive model to predict numerical results for some representative problems in micro-indentation of PMMA, and compare them against corresponding results from physical experiments.

IV. Application to micro-indentation of PMMA

The development of very low-load depth-sensing indentation instruments over the past twenty years or so, which allow one to make indents as shallow as a few nanometers, makes these instruments particularly well-suited for indentation experiments on materials available only in small volumes, such as thin coatings (e.g., [12]; [13]). Since these instruments allow one to continuously record both load, P, down to micro-Newtons, and indentation depths, h, down to nanometers during the indentation cycle, results from such nano/micro-indentation experiments hold the promise of the *in situ* estimation of mechanical properties of materials from the measured P-h curves.

Indentation experiments have long been used to measure the hardness of materials. Interest in instrumented indentation experiments as a means to estimate a wide variety of other mechanical properties (e.g, elastic moduli, yield strength, strain-hardening characteristics, residual stresses, and fracture toughness (for very brittle materials) has grown rapidly in recent years. It is clear from the recent literature (e.g., [14]–[16]) that the problem of estimating material properties from experimentally-measured P-h curves depends crucially on the availability of a large catalog of numerically calculated P-h curves, the attendant details of the time-varying "true projected contact areas", "pile-up/sink-in profiles", and stress and strain distributions in the inhomogeneously-deforming volume of material under the indenter. With a focus on *metallic materials*, most of the recent analyses of indentation (e.g., [16]–[18]) have been performed using a large deformation version of the classical isotropic strain-hardening, rate-independent, elasto-plastic J_2 flow theory. Suresh and co-workers (e.g., [16], [19], [20]) have used the results from such numerical analyses *in conjunction with with suitable scaling relations*[5] to develop a promising methodology for estimating the Young's modulus, yield strength, strain-hardening exponent, as well as the hardness of metallic materials from measured P-h curves in micro-indentation.[6]

A search of the literature reveals that although numerous investigators have conducted nano/micro-indentation experiments to obtain P-h curves for polymeric materials (e.g., [22]–[26]), a corresponding methodology for extracting material property information from the experimental data is not as well developed.[7] This situation for polymeric materials exists primarily because baseline numerical analyses of sharp indentation of polymeric materials using appropriate large deformation constitutive models for the elastic-viscoplastic response of polymeric materials appear not to have been previously reported in the literature. Before one can use experimentally-measured P-h curves from indentation experiments to extract material property information for a given material, *a particular constitutive model must be assumed, the sensitivity of the P-h curves to variation in the values of the constitutive parameters in the model must be studied, and the key material parameters that dominate the P-h response must be determined*. For instance, it is well known that room temperature stress-strain curves obtained from large deformation compression[8] experiments are very sensitive to (a) *the range of strains*: at small strains some amorphous polymers show a strain softening phenomenon, but at large strains they show a very rapid strain-hardening response; (b) *changes in strain path*: polymeric materials exhibit a pronounced Bauschinger effect upon unloading; (c) *the effects of strain rate*: room temperature for polymeric materials is usually not far from their glass-transition or melt temperatures, and they show substantial strain-rate sensitivity of plastic flow; (d) *large hydrostatic pressures*: most amorphous polymeric materials show a sizable positive pressure-sensitivity of the resistance to plastic flow. Without detailed numerical analyses of sharp indentation, it is unclear which of these phenomena significantly affect the P-h curves, and which material properties one can even hope to extract with reasonable accuracy.

A simple, rate-independent, power-law strain-hardening Mises type model, as has been used to simulate the indentation response of metallic materials (e.g., [16], [17]), does not respresent the various physical phenomena — strain-softening and then strain-

[5] Also see [17], [18].

[6] Two of the earliest, and still widely-used, methods for estimating the hardness and Young's modulus (from the maximum load and the initial unloading slope of the P-h curves) are those of [21] and [13].

[7] However, see [27] for a recent attempt.

[8] And also tension experiments on polymers which do not craze.

hardening, Bauschinger effects, strain-rate sensitivity, pressure sensitivity of plastic flow — observed in polymeric materials. A more sophisticated constitutive model which comprehends these effects is needed, and such a model has been developed and calibrated for PMMA in the previous sections of this paper. In this section we check to see if this model can adequately predict the P-h response in sharp-indentation of PMMA with *conical indenters*. Consistent with other researchers, we use a conical indenter with an included angle of 140.6°, which gives the same nominal contact area per unit depth as a Berkovich indenter; i.e. $A = 24.5h^2$, where A is the nominal contact area and h is the indentation depth.

The apparatus for the micro-indentation experiments reported in this paper is the one developed and used by Gearing [28].[9] Details of sample preparation, apparatus calibration, and experimental procedures may be found in [11]. All instrumented indentation experiments were conducted to loads less than 1 N on annealed PMMA at a loading rate of 25 mN/s.

Our constitutive model, as implemented in ABAQUS/Explicit [3], was used to simulate the indentation experiments. Fig. 7 shows the axisymmetric mesh used in the conical-indentation simulations. The section of PMMA modelled is 200 μm tall and has a radius of 400 μm, which is of a sufficiently large size to minimize boundary effects for the $\lessapprox$12 μm indenter penetrations that are expected. The block is meshed with 2940 CAX4R elements, and has a higher density of elements near the indenter tip where most of the deformation takes place. The mesh density was chosen such that at least 15 elements would contact the indenter at the lowest load of 0.16 N.

Using the material parameters for PMMA estimated in the previous section, simulations of conical indentation were conducted at a loading rate of 25 mN/s to loads of 0.16 N, 0.32 N, and 0.64 N. The resulting P-h curves are shown in Fig. 8 along with the experimental results. The numerical predictions of the P-h curves are in very good agreement with the corresponding experiments.

Indentation experiments under load control, which include a "dwell" of 300 seconds at the maximum load were conducted for maximum loads of 0.16 N, 0.32 N, and 0.64 N. The P-h curves showing the expected creep during the dwell period are shown in Fig. 9. The corresponding numerically predicted P-h curves are also shown in this figure. Again, the overall prediction of the P-h curves is in reasonably good agreement with the experiments. Fig. 10 shows details of the dwell depth versus dwell time curves for the three loads. For all loads, the simulations slightly *under-predict* the dwell-creep that is achieved in the experiments. However, overall, the prediction is very respectable.

Fig. 11 shows the P-h curve from another experiment which involves holding the indenter at a given load during the unloading portion of the P-h curve. Note that in this case the creep is in a direction which causes *recovery* of the indentation depth. A numerical simulation of this indentation-recovery experiment is compared with the corresponding experimental result in Fig. 11. In this case, although the model predicts the right trend, it under-predicts the amount of recovery of the indentation depth during the load-hold period. Details of the recovery depth versus time plots are shown in Fig. 12. The numerical simulation for the dwell-recovery experiment does not perform quite as well as those shown for the dwell-creep experiments shown in Fig. 10; the simulation in this case recovers only about 66% of the depth that is observed in the experiment.

V. Conclusions

The constitutive model for amorphous polymeric materials [1] presented in this work differs in considerable detail from previous such models (e.g., [2], [4]–[7]), is quite versatile, and is able to account for the creep response of amorphous glassy polymers at stress levels below those causing "macro-yield", as well as the Bauschinger-type reverse yielding and subsequent zero-load strain recovery phenomena at strain levels less than $\approx 30\%$ associated with the macro-yield transient. While doing so, the model still retains its ability to capture the large strain deformation of this class of materials.

The model has been used to predict the load, P, versus indentation depth, h, response in instrumented micro-indentation experiments on PMMA. Overall, the predictions of the P-h response compare very favorably with corresponding experiments. The model also exhibits the experimentally observed dwell-creep at maximum indentation loads, as well as the dwell-recovery at loads close to complete unloading. However, there is some discrepancy between the actual predicted dwell-recovery versus those that have been experimentally measured. Nevertheless, the results obtained thus far for the micro-indentation predictions are very promising, and may be useful in the future for developing inverse procedures for

[9] Recently, Gearing [28], using the model of [2] (which is a simplified version of the model presented in this paper), has performed detailed numerical analyses of micro-indentation of polymethylmethacrylate, polycarbonate, and polystyrene and developed an approximate method to estimate the Young's modulus, flow strength, rate sensitivity parameter, and pressure sensitivity parameter for an elastic-perfectly-plastic type constitutive model from P-h curves obtained from instrumented indentation experiments. The work presented in this paper is an attempt to better predict the micro-indentation response of PMMA in comparison to that reported in [28], and serve as a verification of the predictive quality of our new constitutive model for engineering applications. The development of an inverse method to estimate material parameters for our new model from instrumented indentation P-h curves is left for future work.

estimating material properties of glassy polymers from nano/micro-indentation experiments.

ACKNOWLEDGMENT

This work was supported by the Singapore MIT Alliance.

REFERENCES

[1] L. Anand, "A finite deformation internal variable model for the visco-elastic-plastic response of amorphous polymers," *in preparation*, 2003.

[2] L. Anand and M. E. Gurtin, "A theory of amorphous solids undergoing large deformations, with application to polymeric glasses," *International Journal of Solids and Structures*, vol. 40, no. 6, pp. 1465–1487, 2003.

[3] ABAQUS, Inc., "ABAQUS Reference Manuals," Pawtucket, RI, 2002.

[4] D. M. Parks, A. S. Argon, and B. Bagepalli, "Large elastic-plastic deformation of glassy polymers, part 1: Constitutive modelling," MIT, Program in Polymer Science and Technology Report, Tech. Rep., 1985.

[5] M. C. Boyce, D. M. Parks, and A. S. Argon, "Large inelastic deformation of glassy polymers. part 1: Rate-dependent constitutive model," *Mechanics of Materials*, vol. 7, pp. 15–33, 1998.

[6] E. M. Arruda and M. C. Boyce, "Evolution of plastic anisotropy in amorphous polymers during finite straining," *International Journal of Plasticity*, vol. 9, pp. 697–720, 1993.

[7] P. D. Wu and E. van der Giessen, "On improved network models for rubber elasticity and their applications to orientation hardening of glassy polymers," *Journal of the Mechanics and Physics of Solids*, vol. 41, pp. 427–456, 1993.

[8] E. Kröner, "Allgemeine kontinuumstheorie der versetzungen und eigenspannungen," *Archive for Rational Mechanics and Analysis*, vol. 4, pp. 273–334, 1960.

[9] E. H. Lee, "Elastic plastic deformation at finite strain," *ASME Journal of Applied Mechanics*, vol. 36, pp. 1–6, 1969.

[10] O. A. Hasan, "An experimental and analytical investigation of the thermomechanical properties of glassy polymers," Ph.D. dissertation, Massachusetts Institute of Technology, 1994.

[11] N. M. Ames, "An internal variable theory for isotropic visco-elastic-plastic solids: Application to indentation of amorphous polymeric solids," Master's thesis, Massachusetts Institute of Technology, 2003.

[12] J. B. Pethica, R. Hutchings, and W. C. Oliver, "Hardness measurements at penetration depths as small as 20 nm," *Philosophical Magazine A*, vol. 48, pp. 593–606, 1983.

[13] W. C. Oliver and G. M. Pharr, "An improved technique for determining hardness and elastic modulus using load and displacement sensing indentation experiments," *Journal of Materials Research*, vol. 7, pp. 1564–1583, 1992.

[14] A. E. Giannakopolous, P. L. Larsson, and R. Vestergaard, "Analysis of vickers indentation," *International Journal of Solids and Structures*, vol. 31, pp. 2679–2708, 1994.

[15] P. L. Larsson, A. E. Giannakopolous, E. Soderlund, D. J. Rowcliffe, and R. Vestergaard, "Analysis of berkovich indentation," *International Journal of Solids and Structures*, vol. 33, pp. 221–248, 1996.

[16] M. Dao, N. Chollacoop, K. J. Van-Vliet, T. A. Venkatesh, and S. Suresh, " Computational modeling of the forward and reverse problems in instrumented sharp indentation," *Acta Materialia*, vol. 49, pp. 3899–3918, 2001.

[17] Y. T. Cheng and C. M. Cheng, "Scaling approach to conical indentation of elastic-plastic solids with work-hardening," *Journal of Applied Physics*, vol. 84, pp. 1284–1291, 1998.

[18] ——, "Scaling relationships in conical indentation of elastic-perfectly plastic solids," *International Journal of Solids and Structures*, vol. 36, pp. 1231–1243, 1999.

[19] A. E. Giannakopolous and S. Suresh, "Determinantion of elasto-plastic properties by instrumented sharp indentation," *Scripta Materialia*, vol. 40, pp. 1191–1198, 1999.

[20] T. A. Venkatesh, K. J. Van-Vliet, A. E. Giannakopolous, and S. Suresh, " Determination of elasto-plastic properties by instrumented sharp indentation: guidelines for property extraction," *Scripta Materialia*, vol. 42, pp. 833–839, 2000.

[21] M. F. Doerner and W. D. Nix, "A method for interpreting the data from depth-sensing indentation instruments," *Journal of Materials Research*, vol. 1, pp. 601–609, 1986.

[22] B. J. Briscoe, L. Fiori, and E. Pelillo, "Nano-indentation of polymeric surfaces," *Journal of Physics, D: Applied Physics*, vol. 31, pp. 2395–2405, 1998.

[23] B. J. Briscoe and K. S. Sebastian, "The elastoplastic response of poly(methyl methacrylate) to indentation," *Proceedings of the Royal Society of London, A*, vol. 452, pp. 439–457, 1996.

[24] R. H. Ion, H. M. Pollock, and C. Roques-Carmes, "Micron-scale indentation of amorphous and drawn PET surfaces," *Journal of Materials Science*, vol. 25, no. 2B, pp. 1444–1454, 1990.

[25] M. R. Van Landingham, J. S. Villarrubia, W. F. Guthrie, and G. F. Meyers, "Nanoindentation of polymers: an overview," in *Recent Advances in Scanning Probe Microscopy, Proceedings of the 220th American Chemical Society National Meeting, August 2000*, V. V. Tsukruk and N. D. Spencer, Eds. Washington D. C.: Wiley-VCH Verlag GmbH, 2001, pp. 15–43.

[26] H. G. H. van Melick, O. F. J. T. Bressers, J. M. J. den Toonder, L. E. Govaert, and H. E. H. Meijer, "A micro-indentation method for probing the craze-initiation stress in glassy polymers," *Polymer*, vol. 44, pp. 2481–2491, 2003.

[27] R. Rikards, A. Flores, F. Ania, V. Kushnevski, and F. Balta-Calleja, "Numerical-experimental method for identification of plastic properties of polymers from microhardness tests ," *Computational Materials Science*, vol. 11, pp. 233–244, 1998.

[28] B. P. Gearing, "Constitutive equations and failure criteria for amorphous polymeric solids," Ph.D. dissertation, Massachusetts Institute of Technology, 2002.

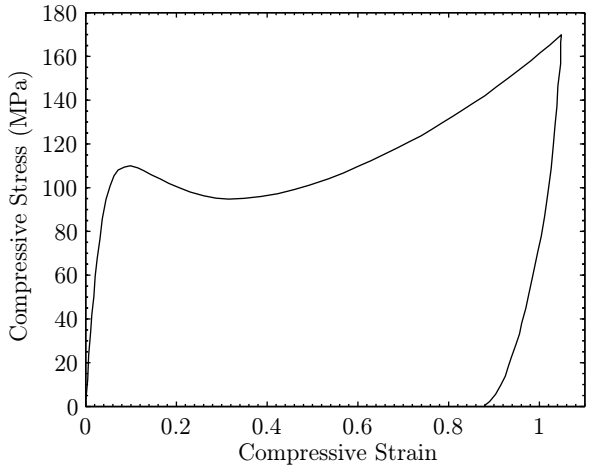

Fig. 1. Simple compression experiment on annealed PMMA at 296 K and a constant true strain rate of -0.001 s^{-1}; from Hasan [10].

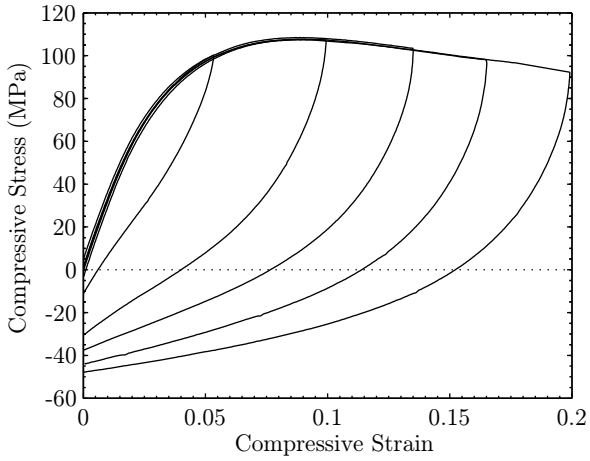

Fig. 2. Compression-tension experiments on annealed PMMA at room temperature at a strain rate of 0.0003 s^{-1}, showing a strong Bauschinger phenomenon. Each curve represents a separate specimen.

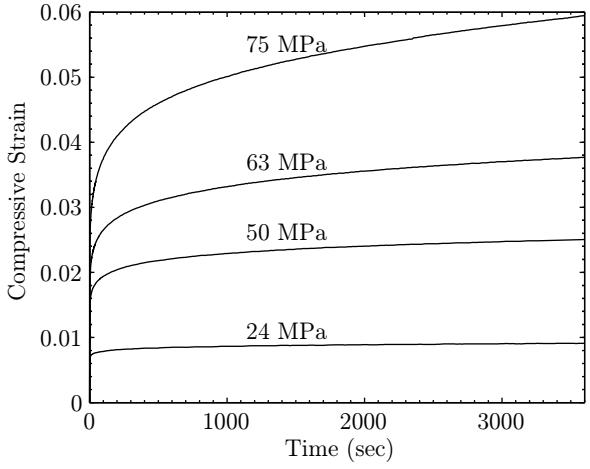

Fig. 3. Compression creep curves from experiments at various pre-macro-yield loads on annealed PMMA at room temperature. Each curve represents a separate specimen.

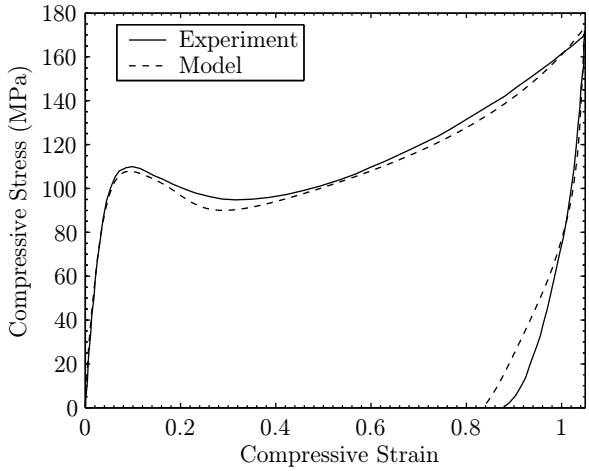

Fig. 4. Comparison of numerical stress-strain curve for large-strain compression against a corresponding experimental result.

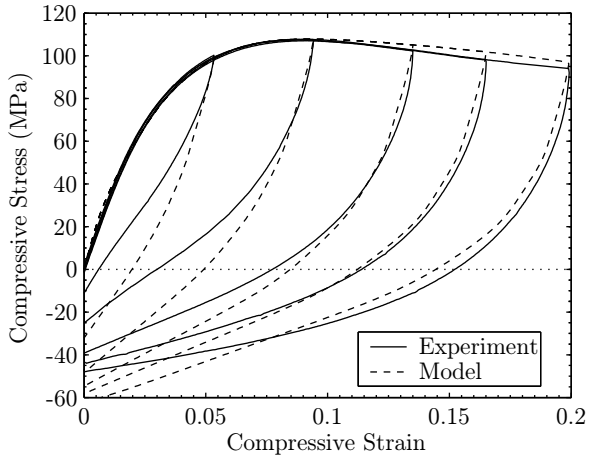

Fig. 5. Comparison of numerical stress-strain curves for compression-tension experiments against corresponding experimental results.

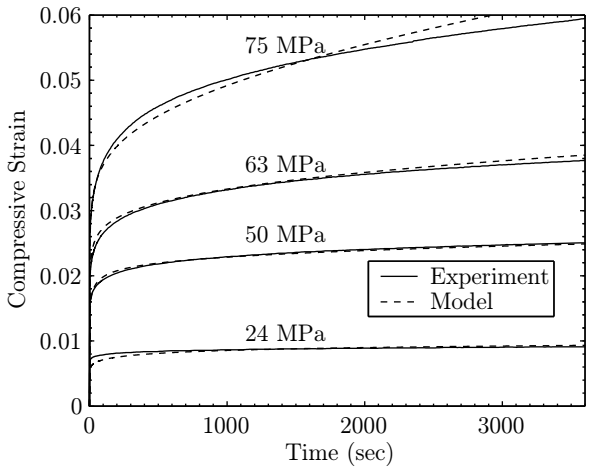

Fig. 6. Comparison of numerical compression creep curves against corresponding experimental results.

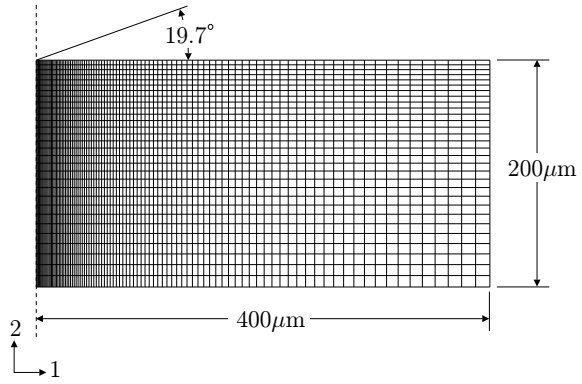

Fig. 7. Finite element mesh for axisymmetric conical indentation used in simulations.

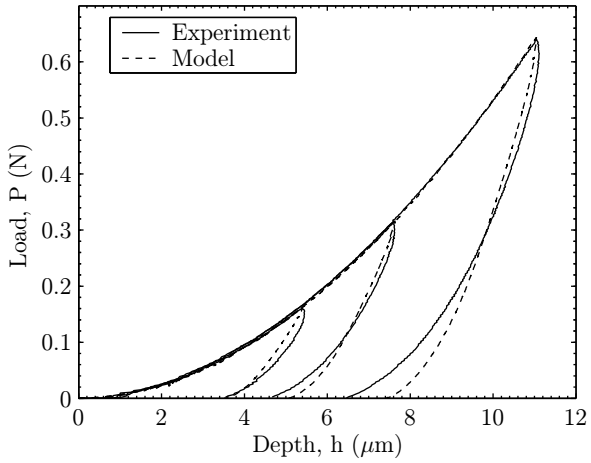

Fig. 8. Comparison of P-h curves from micro-indentation simulations against corresponding experimental results. Maximum loads: 0.64 N, 0.32 N, and 0.16 N.

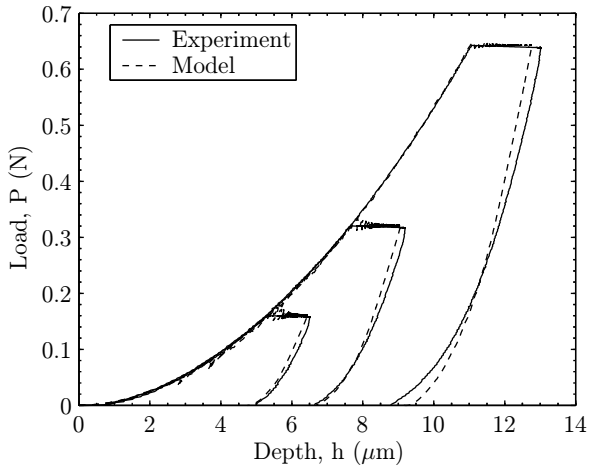

Fig. 9. Comparison of P-h curves from micro-indentation simulations against corresponding experimental results which include a dwell period of 300 seconds at maximum loads of 0.64 N, 0.32 N, and 0.16 N.

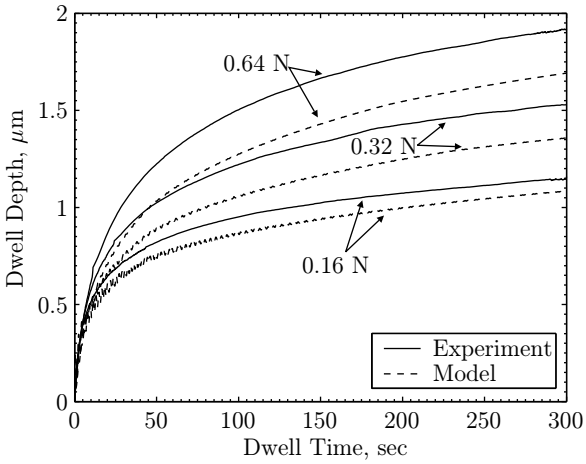

Fig. 10. Detailed comparison of numerically-predicted dwell-creep against corresponding experimental results of Fig. 9.

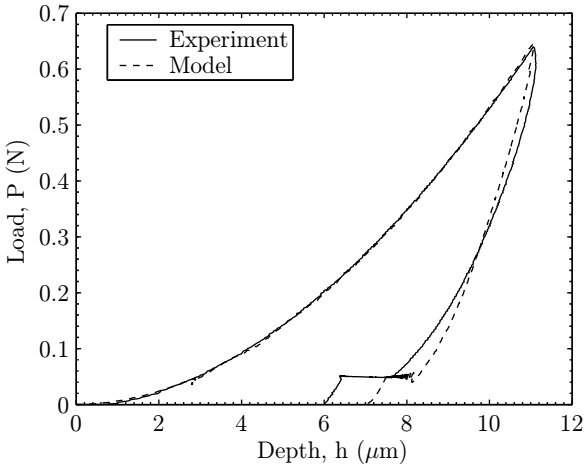

Fig. 11. Comparison of P-h curves from micro-indentation simulation against corresponding experimental results which include a dwell period of 300 seconds at load of 0.05N during the unloading portion of the P-h curve.

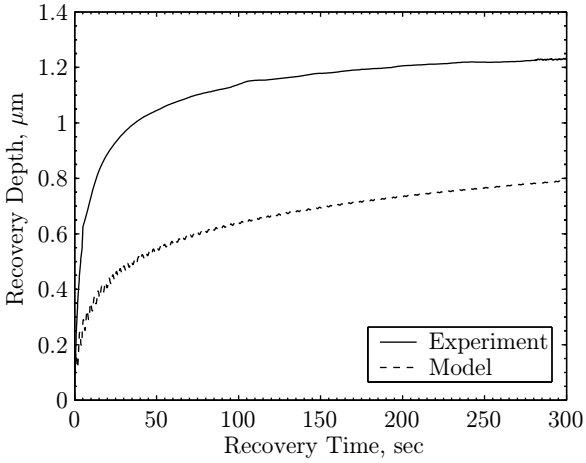

Fig. 12. Detailed comparison of numerically-predicted dwell-recovery against corresponding experimental results of Fig. 11.